# Three-dimensional shapes and distribution of FePd nanoparticles observed by electron tomography using high-angle annular dark-field scanning transmission electron microscopy

Kazuhisa Sato,[1,a)] Kenta Aoyagi,[2] and Toyohiko J. Konno[1]
[1]*Institute for Materials Research, Tohoku University, Sendai 980-8577, Japan*
[2]*Department of Materials Science, Tohoku University, Sendai 980-8579, Japan*

(Received 23 October 2009; accepted 3 December 2009; published online 20 January 2010)

We have studied three-dimensional shapes and distribution of FePd nanoparticles, prepared by electron beam deposition and postdeposition annealing, by means of single-axis tilt tomography using atomic number contrasts obtained by high-angle annular dark-field scanning transmission electron microscopy. Particle size, shape, and locations were reconstructed by weighted backprojection (WBP), as well as by simultaneous iterative reconstruction technique (SIRT). We have also estimated the particle size by simple extrapolation of tilt-series original data sets, which proved to be quite powerful. The results of the two algorithms for reconstruction have been compared quantitatively with those obtained by the extrapolation method and those independently reported by electron holography. It was found that the reconstructed intensity map by WBP contains a small amount of dotlike artifacts, which do not exist in the results by SIRT, and that the particle surface obtained by WBP is rougher than that by SIRT. We demonstrate, on the other hand, that WBP yields a better estimation of the particle size in the $z$ direction than SIRT does, most likely due to the presence of a "missing wedge" in the original data set. © *2010 American Institute of Physics*. [doi:10.1063/1.3280026]

## I. INTRODUCTION

Recent developments in ultrahigh density magnetic storage technology rely on novel recording media with a high magnetocrystalline anisotropy energy (MAE), in order to increase storage density and to reduce recording noises. FePd alloy nanoparticles with the $L1_0$-type ordered structure is one of the candidate materials suitable for the ultrahigh density magnetic storage media. The hard magnetic properties of these alloy nanoparticles originate from the tetragonal ordered structure, which gives rise to a high MAE,[1,2] and thus the atomic ordering is a key issue for improving the hard magnetic properties of the $L1_0$-type alloy nanoparticles. Therefore previous studies have focused on the atomic structure inside the nanoparticles.[3–5] On the other hand, high-areal density packing of nanoparticles and control of magnetostatic interaction among nanoparticles are considered as the next step to realize ultrahigh density magnetic storage media. For this purpose, it is desired to visualize and understand three-dimensional (3D) shapes of nanoparticles and spatial configuration of neighboring particles precisely. One of the interests here is the height (thickness) and the aspect ratio (height/diameter) of particles from view points of the shape anisotropy of very small nanoparticles. However, in transmission electron microscopy (TEM), an accurate evaluation of the sample height is usually difficult and subject to careful examinations.

Electron tomography, especially its applications to materials science, is a novel technique, which can retrieve 3D structural information usually missing in TEM and scanning TEM (STEM). A 3D structure can be reconstructed by processing a tilt series of electron micrographs with mass-thickness contrasts, formed by several different imaging techniques: bright-field (BF) TEM,[6–8] dark field TEM,[9–11] atomic number (Z) contrast of STEM,[12–14] energy-filtered TEM,[13] and electron holography.[15] The recent progress in this field has been summarized in review articles.[16,17] In all the techniques, acquisition of clear contrast images and accurate alignments of the sample position and/or the tilt axis are essential for subsequent 3D reconstruction. Some model simulations on the accuracy of reconstruction have been presented in detail.[13] Quantitative analyses have revealed the complex 3D structures of nanoporous gold.[18,19] Recent reports have shown, for example, facetted surfaces in reconstructed Pt nanoparticles[20] or Pd nanoparticles.[21] Alloyeau *et al.*[22] have carried out a quantitative thickness analysis of CoPt nanoparticles by comparing a focal series of high-resolution TEM (HRTEM) images with the reconstructed 3D structures of BF-TEM tilt series. As demonstrated by them, an investigation for a novel method to quantify 3D reconstructed structures is one of the fundamental interests in the electron tomography.

In this study we have examined 3D shapes and distributions of $L1_0$-FePd alloy nanoparticles epitaxially grown on the single crystal NaCl(001) substrate by means of electron tomography using Z-contrast of high-angle annular dark-field (HAADF) STEM. The Z-contrast can be regarded as a suitable mass-thickness contrast required for electron tomography, where incoherent imaging is dominant with negligible contribution of diffraction contrasts. We compare, in a semi-quantitative manner, the accuracy of thickness of the nano-

[a)]Author to whom correspondence should be addressed. Electronic mail: ksato@imr.tohoku.ac.jp.

 

particles deduced by different reconstruction techniques using a tilt-series data set of HAADF-STEM images of the FePd nanoparticles.

## II. EXPERIMENTAL PROCEDURES

FePd nanoparticles were fabricated by sequential electron beam deposition of Pd and Fe onto a NaCl(001) substrate at 673 K.[3,4] After deposition of Fe, an amorphous $Al_2O_3$ thin film was deposited to protect the particles from oxidation. The as-deposited specimen film was then removed from the NaCl substrate by immersing the substrate into distilled water, and was mounted onto conventional copper grids for STEM observation. Postdeposition annealing of the as-deposited film on a copper grid at 873 K for 3.6 ks led to the formation of the $L1_0$-type ordered structure in FePd nanoparticles.[23] The mean cooling rate after the annealing was about 10 K/min. The orientation relationship between FePd islands and the NaCl substrate, as confirmed by electron diffraction, is $\langle 001\rangle_{FePd}\|\langle 001\rangle_{NaCl}$, $\{100\}_{FePd}\|\{100\}_{NaCl}$. The average alloy composition was Fe-49 at. % Pd according to the results of energy dispersive x-ray spectroscopy. Details of the atomic structures of FePd nanoparticles have been described in our previous articles.[3–5,23]

Z-contrast STEM images were obtained using an FEI Titan 80–300 (S)TEM operating at 300 kV with a field emission gun. We set the beam convergence to be 10–14 mrad in half-angle, taking into account the spherical aberration coefficient (1.2 mm) of the prefield of objective lens. The tilt series of Z-contrast images were acquired by using a HAADF-detector (Fischione model 3000) with the inner angle higher than 60 mrad. The XPLORE3D software (FEI Co. Ltd) was used for data sets acquisition taking the dynamic focus into consideration. A single-tilt holder (Fischione model 2020) and a triple-axes holder (Mel-Build model HATA-8075) were used for the tilt-series acquisition with the maximum tilt angle of 70°. Alignment of the tilt axis for the obtained data set by an iterative cross-correlation technique and subsequent 3D reconstruction were performed by using the INSPECT3D software package (FEI Co. Ltd). As for the algorithm for 3D reconstruction, we employed weighted backprojection (WBP),[24] as well as simultaneous iterative reconstruction technique (SIRT).[25] The reconstructed 3D density data were then visualized using the AMIRA 4.1 software (Visage Imaging).

## III. RESULTS AND DISCUSSION

Figure 1 shows Z-contrast images acquired during a tilt-series observation, after tilt-axis correction. The tilt series was observed sequentially from 0° to −70° and then 0° to +70°. The tilt angle increments were set 2° for angle ranges of 0° to |50|° and 1° for |50|° to |70|°. Out of this data set, we employed, by careful inspection of contrasts, images taken at tilt angles between −66° and +64° for later 3D reconstruction. These tilt angles and increments are in a typical range usually employed in the single tilt-axis STEM HAADF electron tomography.[8,13,16,21] Large particles of bright contrasts about 30 nm in size, as indicated by arrows in Figs. 1(b) and 1(c), are Cu particles later deposited onto the specimen film. The reconstructed volume, $75\times75$ nm$^2$ in size and 36 nm in depth, is also indicated in Fig. 1(a).

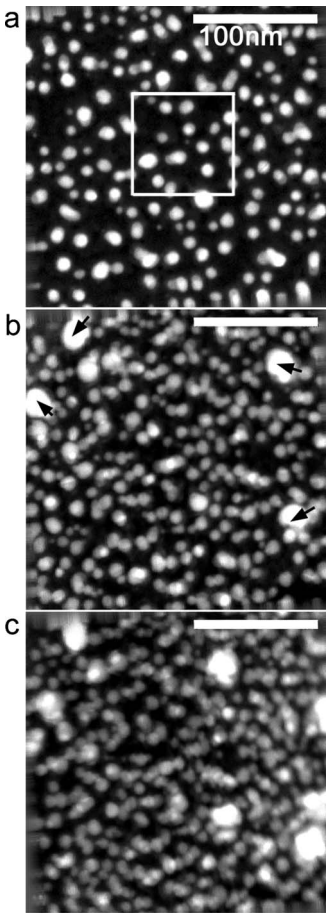


FIG. 1. Z-contrast images acquired during a tilt-series observation, after tilt-axis correction. (a) $\alpha$=0°, (b) $\alpha$=−66°, and (c) $\alpha$=+64°. The tilt series was observed sequentially from 0° to −70° and then 0° to +70°. The reconstructed area, $75\times75$ nm$^2$ in size, is also indicated in Fig. 1(a). Large Cu particles are indicated by arrows in Fig. 1(b).

Figure 2 compares an original image [Fig. 2(a)] and corresponding reconstructed images processed by WBP [Fig. 2(b)] and SIRT [Fig. 2(c)], viewed along the $z$ axis, which is parallel to the beam incidence direction. The tilt axis is the $x$ axis, about which the specimen film is sequentially tilted toward the $y$ direction. As seen, general features, such as particle shape, size, and location, projected onto $x$-$y$ plane, are clearly reconstructed in Figs. 2(b) and 2(c), irrespective of the algorithm. However, it is noted that some floating dotlike artifacts, as indicated by the arrows, are seen in the reconstructed image obtained with WBP [Fig. 2(b)], while the result by the SIRT shows a smooth surface with little apparent artifacts.

The reconstructed result using WBP is shown in Fig. 3 with $x$-$y$ (plan-view), $y$-$z$, and $z$-$x$ (side-view) projections. All the nanoparticles exist on the same plane, namely the substrate surface because they grew epitaxially on a single crystal substrate. The particle growth direction is in the $z$ direction as indicated. As seen, the particle shape is rather oblate characterized by a diameter longer than thickness. Here the term, particle thickness or height, is defined as the

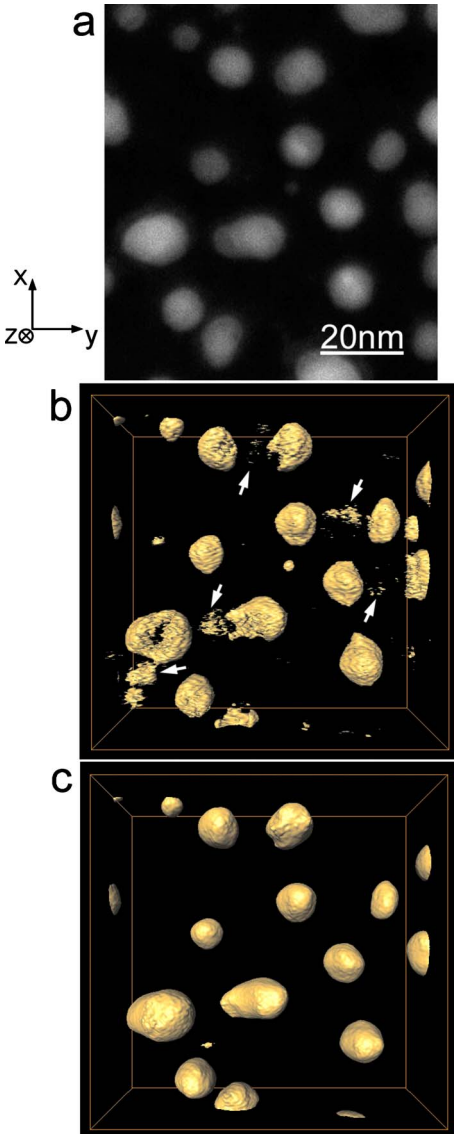


FIG. 2. (Color online) An original image (a), corresponding reconstructed images processed by WBP (b) and SIRT (c), viewed along the $z$ axis, which is parallel to the beam incidence direction. Arrows in (b) indicate floating dotlike artifacts. The tilt axis is the $x$ axis, about which the specimen film is sequentially tilted.

distance from the bottom to the top surfaces of a nanoparticle in the $z$ direction. Also dotlike artifacts are seen in the $y$-$z$ and the $z$-$x$ projections. These artifacts can be minimized by adjusting a threshold value of the visualizing software (AMIRA), although it ended up making a hole inside a nanoparticle as indicated by arrows in the $x$-$y$ projection. When the threshold value was so set that all these floating artifacts are gone, it was found that some of the fine details of nanoparticles also diminish. This observation suggests that there exists a best condition of the threshold value for reconstructing the shapes of nanoparticles without influencing their sizes. This criterion can be employed in a reliable manner by comparing them with original Z-contrast images. In fact, these subtleties of the optimization procedure led us to a conclusion that the small amounts of floating artifacts cannot be eliminated in the WBP method.

In contrast, SIRT gives a clear 3D morphology as shown in Fig. 4. Besides the absence of floating artifacts, significant differences between Figs. 3 and 4 can be noticed. For example, particle surface appears smooth in SIRT images. It can be noticed that particle heights, i.e., particle lengths in the $z$ direction, shown in Fig. 4, are apparently longer than those in Fig. 3. Indeed SIRT gave particle heights, which are almost comparable to or even longer than the particle diameter, while rather flat 3D shapes can be seen in the result by WBP (Fig. 3). The difference in the aspect ratio of the reconstructed results is pronounced when viewed from an oblique direction as shown in Fig. 5. Nanoparticles in the upper image (WBP) show oblate 3D-shapes, while those in the lower images (SIRT) are prolate, i.e., elongated in the $z$ direction.

When considering the resolution of a reconstructed structure in electron tomography, a proper alignment of the tilt axis of a data set is necessary prior to reconstruction. To satisfy this fundamental requirement, we followed the standard alignment procedure based on cross-correlation. Besides, there exist two kinds of factors that may affect the accuracy of reconstruction. One is a finite number of two-dimensional (2D)-slice images due to a discrete image acqui-

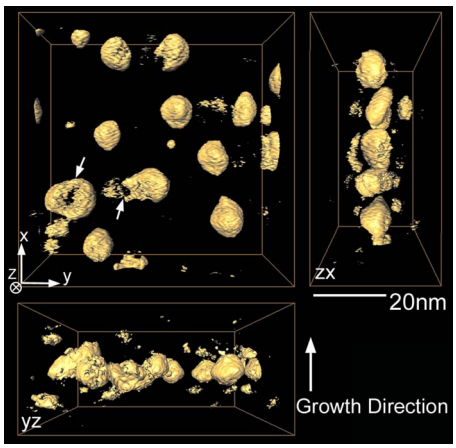


FIG. 3. (Color online) Reconstructed result of the FePd nanoparticles processed by WBP. The reconstructed volume is $75 \times 75 \times 36$ nm$^3$. Arrows in the $x$-$y$ projection indicate the artifacts (hole) inside the nanoparticles. Particle growth direction is also indicated in the $y$-$z$ projection.

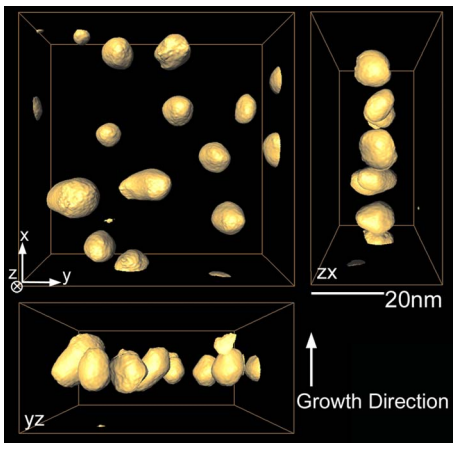


FIG. 4. (Color online) Reconstructed images of the FePd nanoparticles processed by SIRT with 20 iterations. The reconstructed volume is identical to that processed by WBP shown in Fig. 3. SIRT gives a clear 3D morphology without the floating artifacts.

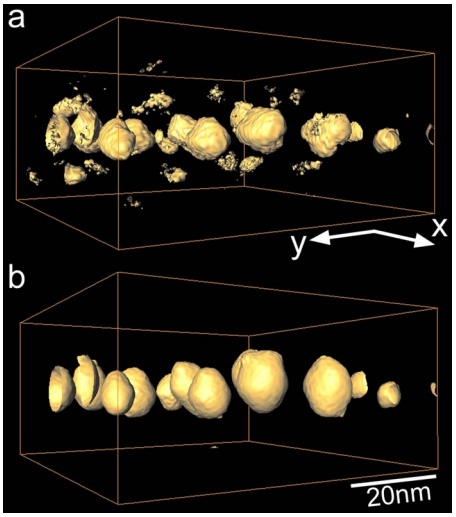


FIG. 5. (Color online) Oblique-view of the reconstructed volume processed by (a) WBP (upper) and (b) SIRT (lower). Large discrepancy in particle thickness (height) is apparent between these two images. Nanoparticles in the upper image show oblate 3D-shapes, while those in the lower images are prolate. The reconstructed volume is $75\times75\times36$ nm$^3$.

sition and the other is a maximum tilt angle limited by the pole-piece design of a microscope. These points have been summarized in the recent article by Midgley and Weyland.[13] In the framework of single-axis tilt geometry, the resolution along $x$, $y$, and $z$ directions are all different. The resolution along the tilt axis ($x$ axis) corresponds to the resolution of the microscope and therefore the highest resolution is expected in this direction. On the other hand, the resolution along the $y$ and $z$ axes, $d_y$ and $d_z$, respectively, are expressed as follows:[24,26,27]

$$d_y = \frac{\pi D}{N}, \tag{1}$$

$$d_z = d_y e_{yz}, \tag{2}$$

$$e_{yz} = \sqrt{\frac{\alpha + \sin\alpha\cos\alpha}{\alpha - \sin\alpha\cos\alpha}}, \tag{3}$$

where $N$, $D$, and $\alpha$ denote the number of images used for reconstruction, the diameter of the reconstructed volume assuming a cylindrical shape (the tilt axis corresponds to the axis of the cylinder), and the tilt angle, respectively. Note that Eq. (1) assumes the tilting range from $-90°$ to $+90°$ with an equal angular increment. Hence it is only an approximation in the case of electron tomography, where tilting range is limited. The parameter $e_{yz}$ is known as an elongation factor, which expresses the effect of a missing data set at high angles on reconstruction. In the present experimental setup, images at tilt angles from $|70|°$ to $|90|°$ cannot be obtained and the information inside this area is thus missing, as often referred to as the missing wedge. The resolution defined by Eqs. (1) and (2), predicts an apparent elongation of the reconstructed image in the $z$ direction. Numerically, we derived the resolution in the present study by applying the experimental parameters [$N=81$, $D=75$ nm, and $\alpha=65°$ (average of $-66°$ and $+64°$)] into Eqs. (1)–(3), which

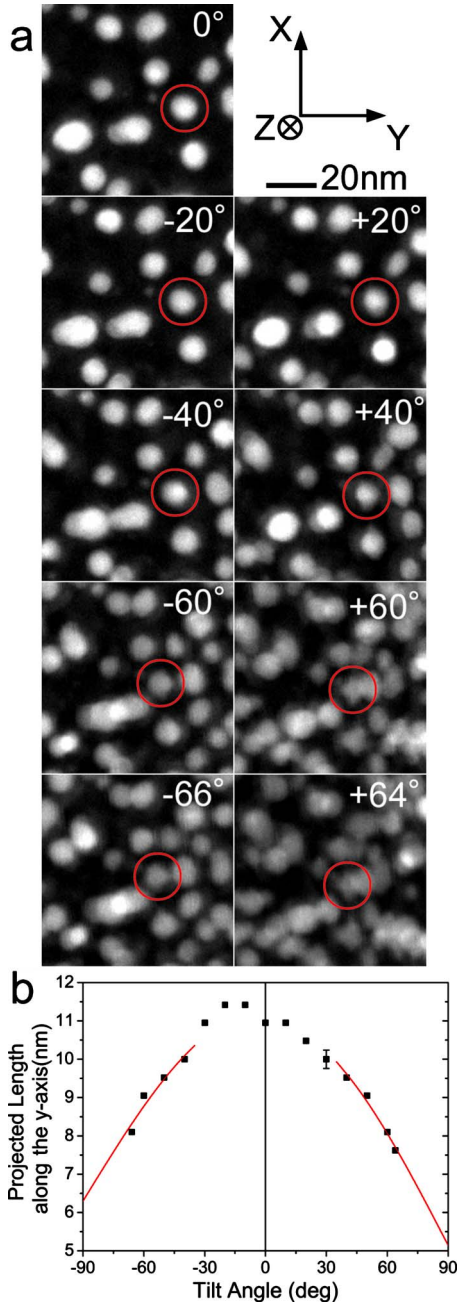


FIG. 6. (Color online) (a) A series of Z-contrast images taken at different tilt angles. (b) The analyzed particle length in the $y$ direction as a function of the tilt angle. The particle length decreases as the tilt angle increases toward 90°, indicating the fact that the particle height is shorter than the diameter. Extrapolation of particle length in the $y$ direction to the value expected at the tilt angle $\alpha=90°$ leads to an elucidation of the true particle height. Here, the extrapolation was performed by fitting the data points at angles higher than 40° using cosine of the tilt angle.

yielded the following values; $d_y=2.9$ nm, $d_z=4.1$ nm with $e_{yz}=1.42$ for reconstructed volume ($xyz$) of $75\times75\times36$ nm$^3$. Thus, a simple estimation predicts possible elongation of the reconstructed image as large as 42%.

Figure 6 shows a series of Z-contrast images taken at different tilt angles. As seen, the apparent particle length in the $y$ direction becomes shorter as the tilting angle increases. A nanoparticle enclosed by the circle in the figure is one of the examples to demonstrate the reduction in the particle image in the $y$ direction. According to our previous study

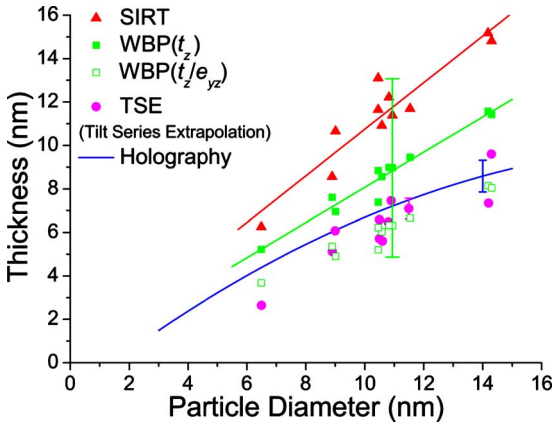


FIG. 7. (Color online) The relation between particle diameter and thickness (height) for the FePd nanoparticles estimated by using several different techniques. The large error bar for WBP indicates a possible elongation of $d_z$ =4.1 nm, as suggested by Eqs. (2) and (3).

using electron holography, it was found that the FePd nanoparticles have flat top surfaces parallel to the substrate plane and possess almost pyramidal shape with curved corners.[3] Quantitative analysis of the interference images also revealed that the particle thickness is about 60% shorter than the particle diameter. If this is the case, the apparent particle length in the $y$ direction, which is the diameter, should decrease with tilting. To examine a possible elongation of a reconstructed particle height in the $z$ direction, we therefore measured projected particle length in the $y$ direction as a function of tilt angle and deduced the true particle height by extrapolating the projected length to the value expected at the tilt angle $\alpha$=90°. The results are plotted in Fig. 6(b). As seen, the projected length clearly decrease with tilting, which indicates that the particle height is actually shorter than the diameter. Note that this simple extrapolation of the raw data led to a result, which agrees well with the previous study using electron holography. Here, the extrapolation was performed by fitting the data points at angles higher than 40° using cosine of the tilt angle because of the fact that the projected $y$ length is proportional to cos $\alpha$ at high angles when the particle height is shorter than the diameter.

Using the aforementioned procedure, here termed "tilt-series extrapolation (TSE) method" in the present paper, we obtained a relation, which summarizes the relation between particle diameter and thickness estimated by using several different techniques (Fig. 7). Solid triangles and solid squares indicate the results obtained from the reconstructed images based on SIRT and WBP, respectively. The large error bar for WBP indicates a possible elongation of $d_z$ =4.1 nm, as suggested by Eqs. (2) and (3). Therefore, we divided the apparent particle thickness ($t_z$), which was deduced from the 3D volumes based on WBP, by the elongation factor ($e_{yz}$=1.42) for the present experimental condition. The results, $t_z/e_{yz}$, are indicated by open squares. It should be mentioned here that the validity of the $t_z/e_{yz}$ has been demonstrated by comparing the measured thickness based on the WBP with those deduced from the focal series of HR-TEM images.[22] Solid circles denote the deduced particle thickness measured from the TSE method. A solid curve indicates the previous result based on the electron holography.[3] Note that the deduced thicknesses obtained by the TSE agree well with those obtained by WBP ($t_z/e_{yz}$) as well as those by electron holography. On the other hand, the thicknesses suggested by SIRT are much larger than the values deduced by the TSE method or electron holography. In contrast, the apparent thickness predicted by WBP is close to the deduced values with an error of about 1–4 nm in thickness, without taking the elongation factor into consideration. Therefore, within a framework of single-axis tilt geometry, it is demonstrated in a semiquantitative manner that the WBP gives a better result in terms of the accuracy of the particle length in the $z$ direction than that predicted by SIRT, despite the fact that the latter algorithm is superior to the former from the viewpoints of artifacts.

In the present study, 20 iterations were carried out in SIRT to minimize the differences between the original projected series and the calculated ones. Because of the iterative and direct-methodological natures of the SIRT, which does not use Fourier transformation, the resolution defined by Eqs. (1)–(3) cannot be directly applied to the reconstructed results by SIRT. It has been demonstrated that the SIRT reconstructions converge after about ten cycles of iteration.[25] Our examination also suggested that the particle thickness remained fairly constant even after large number of iterations up to 50 cycles. We have also observed that the surface of the reconstructed nanoparticles become rather rough after 30–50 cycles compared to that of the 20 cycles. A quite small increase in the particle thickness, corresponding to only one to two pixels (less than 0.5 nm), was recognized for the results after five to ten cycles. Therefore, 20 cycles of iterations were considered appropriate for the reconstruction in the present study. Indeed, Aronova *et al.*[28] have pointed out the existence of an optimal number of iterations when raw data sets contain Poisson noise. They employed 20–30 iterations for SIRT. Similar tendency was also reported in a study by Tong *et al.*[29] To summarize, the present comparison demonstrated that, 3D structural information of the nanoparticles can be refined during the iteration process, however, at the same time, it also showed that artifacts in the $z$ direction due to the existence of a missing wedge cannot be effectively removed during the iterations, leading to an apparent elongation of particles in the $z$ direction. The reason for this artifact is not clear at this moment. To reduce the artifacts, a minimization of the missing wedge will be most effective, which can be attained by increasing the maximum tilt angle together with number of 2D-slice images as possible. For this purpose, dedicated future studies, including dual-axis tomography,[29,30] will be necessary.

Finally, we applied 3D tomography in order to elucidate spatial configuration of as-deposited Fe/Pd nanocomplex particles. A tilt series of Z-contrast images were acquired using a triple-axes holder with tilting angles of −70° to +66° at 2° increments and reconstruction was carried out using SIRT with 20 iterations. Z-contrast image shown in Fig. 8(a) includes two kinds of contrast regions: bright regions corresponding to nanoparticles and weak contrast regions between neighboring particles, as indicated by the arrows. According to our previous study,[23] as-deposited bcc-Fe particles were

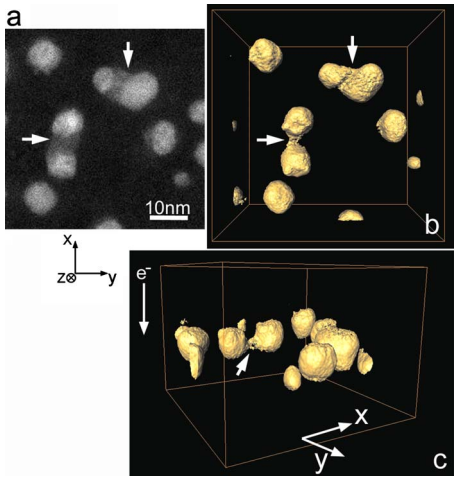


FIG. 8. (Color online) Results of the tomographic reconstruction for the as-deposited Fe/Pd nanoparticles. (a) An original Z-contrast image, (b) reconstructed volume (*x*-*y* plane), and (c) that of viewed in an oblique direction.

found to epitaxially grow onto fcc-Pd islands, which had been grown epitaxially on the NaCl(001) substrate. Thus, the weak contrast region is likely to arise from unalloyed Fe because of the sequential deposition of Fe onto Pd nanoparticles. The rather weak contrast seen between the neighboring particles indicates that only a small amount of Fe exists here. The 3D reconstruction revealed that these unalloyed Fe regions between the neighboring Pd particles locate at the bottom side of the nanoparticles as indicated by the arrow in Fig. 8(c). This observation hence demonstrates that STEM-tomography can be used to understand the spatial configuration of partially coalesced nanoparticles, and the mechanism of alloy formation clearly.

## IV. SUMMARY

We have studied 3D shapes and spatial configuration of 10 nm sized FePd nanoparticles by means of single-axis tilt tomography using HAADF-STEM images obtained in the tilting range of $-66°$–$+64°$. The algorithms employed for reconstruction were WBP and SIRT and the resultant 3D information was compared with those estimated by the TSE method, and those obtained by the previous holographic study. Main results are summarized as follows:

(1) Floating dotlike artifacts were observed in the image reconstructed by WBP, while SIRT can reproduce smooth surface with no apparent floating artifacts.
(2) Estimated resolution of the reconstructed size by WBP was 2.9 and 4.1 nm for the *y* direction (perpendicular to the tilt axis) and the *z* direction, respectively, based on the number of 2D-slices, size of the reconstructed volume ($75\times75\times36$ nm$^3$), and the maximum tilt angle.
(3) The particle size in the *z* direction was examined quantitatively. The results by TSE agree well with those obtained by WBP as well as electron holography, while SIRT led to an overestimation of 3–8 nm, indicating that SIRT is more prone than WBP to the overmeasure of particle size in the *z* direction, when data in a certain angular region are missing.
(4) The above results suggest that, during the iteration of SIRT, structural information, including 3D surface morphology, can be refined; while artifacts in the estimation of the size in the *z* direction cannot be effectively reduced within the present experimental setup or conditions.
(5) It is also demonstrated that a method based on a simple extrapolation of a raw data set, referred to here as TSE method, is found to be reliable and useful, in order to examine the accuracy and resolution of 3D reconstructed information provided by different algorithms.

## ACKNOWLEDGMENTS

This study was partially supported by the Grant-in-Aid for Young Scientists (B) (Grant No. 19760459) from the Ministry of Education, Culture, Sports, Science, and Technology, Japan. K.S. acknowledges the financial support from the Kazato Research Foundation. Electron microscopy was carried out in the High-Voltage Electron Microscope Laboratory, Tohoku University. The authors wish to thank Emeritus Professor Y. Hirotsu of Osaka University for invaluable comments and Dr. K. Inoke of FEI Co. Japan Ltd., Mr. E. Aoyagi, and Mr. Y. Hayasaka of Tohoku University for their help using TEM.

[1]D. Weller and M. F. Doerner, Annu. Rev. Mater. Sci. **30**, 611 (2000).
[2]H. Shima, K. Oikawa, A. Fujita, K. Fukamichi, K. Ishida, and A. Sakuma, Phys. Rev. B **70**, 224408 (2004).
[3]K. Sato, Y. Hirotsu, H. Mori, Z. Wang, and T. Hirayama, J. Appl. Phys. **98**, 024308 (2005).
[4]K. Sato, T. J. Konno, and Y. Hirotsu, J. Appl. Phys. **105**, 034308 (2009).
[5]K. Sato, J. G. Wen, and J. M. Zuo, J. Appl. Phys. **105**, 093509 (2009).
[6]M. Shirai, T. Horiuchi, A. Horiguchi, S. Matsumura, K. Yasuda, M. Watanabe, and T. Masumoto, Mater. Trans. **47**, 52 (2006).
[7]K. Kaneko, R. Nagayama, K. Inoke, E. Noguchi, and Z. Horita, Sci. Technol. Adv. Mater. **7**, 726 (2006).
[8]T. Mizoguchi and U. Dahmen, Philos. Mag. Lett. **89**, 104 (2009).
[9]K. Kimura, S. Hata, S. Matsumura, and T. Horiuchi, J. Electron Microsc. **54**, 373 (2005).
[10]J. S. Barnard, J. Sharp, J. R. Tong, and P. A. Midgely, Science **313**, 319 (2006).
[11]S. Hata, K. Kimura, H. Gao, S. Matsumura, M. Doi, T. Moritani, J. S. Barnard, J. R. Tong, J. H. Sharp, and P. A. Midgley, Adv. Mater. **20**, 1905 (2008).
[12]U. Ziese, C. Kübel, A. J. Verkleij, and A. J. Koster, J. Struct. Biol. **138**, 58 (2002).
[13]P. A. Midgley and M. Weyland, Ultramicroscopy **96**, 413 (2003).
[14]K. Kaneko, K. Inoke, K. Sato, K. Kitawaki, H. Higashida, I. Arslan, and P. A. Midgley, Ultramicroscopy **108**, 210 (2008).
[15]A. C. Twitchett, T. J. V. Yates, R. E. Dunin-Borkowski, S. B. Newcomb, and P. A. Midgley, J. Phys.: Conf. Ser. **26**, 29 (2006).
[16]C. Kübel, A. Voigt, R. Schoenmakers, M. Otten, D. Su, T. C. Lee, A. Carlsson, and J. Bradley, Microsc. Microanal. **11**, 378 (2005).
[17]P. A. Midgley and R. E. Dunin-Borkowski, Nature Mater. **8**, 271 (2009).
[18]H. Rösner, S. Parida, D. Kramer, C. A. Volkert, and J. Weissmüller, Adv. Eng. Mater. **9**, 535 (2007).
[19]T. Fujita, L. H. Qian, K. Inoke, J. Erlebacher, and M. W. Chen, Appl. Phys. Lett. **92**, 251902 (2008).
[20]L. C. Gontard, R. E. Dunin-Borkowski, M. H. Gass, A. L. Bleloch, and D. Ozkaya, J. Electron Microsc. **58**, 167 (2009).
[21]S. Benlekbir, T. Epicier, M. Bausach, M. Aouine, and G. Berhault, Philos. Mag. Lett. **89**, 145 (2009).
[22]D. Alloyeau, C. Ricolleau, T. Oikawa, C. Langlois, Y. Le Bouar, and A. Loiseau, Ultramicroscopy **109**, 788 (2009).
[23]K. Sato and Y. Hirotsu, J. Appl. Phys. **93**, 6291 (2003).
[24]M. Radermacher, in *Electron Tomography: Three-Dimensional Imaging*

*with the Transmission Electron Microscope*, edited by J. Frank (Plenum, New York, 1992).
[25]P. Gilbert, J. Theor. Biol. **36**, 105 (1972).
[26]R. A. Crowther, D. J. DeRosier, and A. Klug, Proc. R. Soc. London, Ser. A **317**, 319 (1970).
[27]M. Radermacher, J. Electron Microsc. Tech. **9**, 359 (1988).
[28]M. A. Aronova, Y. C. Kim, R. Harmon, A. A. Sousa, G. Zhang, and R. D. Leapman, J. Struct. Biol. **160**, 35 (2007).
[29]J. Tong, I. Arslan, and P. Midgley, J. Struct. Biol. **153**, 55 (2006).
[30]I. Arslan, J. R. Tong, and P. A. Midgley, Ultramicroscopy **106**, 994 (2006).